Bioactive Materials 6 (2021) 2629–2642

Contents lists available at ScienceDirect

Bioactive Materials

journal homepage: www.sciencedirect.com/journal/bioactive-materials

Ionized jet deposition of antimicrobial and stem cell friendly silver-substituted tricalcium phosphate nanocoatings on titanium alloy

Gabriela Graziani [a,*], Katia Barbaro [b], Inna V. Fadeeva [c], Daniele Ghezzi [a], Marco Fosca [d], Enrico Sassoni [e], Gianluca Vadalà [f], Martina Cappelletti [g], Francesco Valle [h], Nicola Baldini [a,i,j], Julietta V. Rau [d,k]

[a] IRCSS Istituto Ortopedico Rizzoli, Laboratory of NanoBiotechnology, via di Barbiano 1/10 40136, Bologna, Italy
[b] Istituto Zooprofilattico Sperimentale Lazio e Toscana "M. Aleandri", Via Appia Nuova 1411-00178, Rome, Italy
[c] A.A. Baikov Institute of Metallurgy and Materials Science, Russian Academy of Sciences, Leninsky prospect 49, 119334, Moscow, Russia
[d] Istituto di Struttura della Materia, Consiglio Nazionale delle Ricerche (ISM-CNR), Via del Fosso del Cavaliere, 100 – 00133, Rome, Italy
[e] University of Bologna, Department of Civil, Chemical, Environmental and Materials Engineering, via Terracini 28 40131, Bologna, Italy
[f] Università Campus Bio-Medico di Roma, Research Unit of Orthopaedic Surgery, Faculty of Medicine and Surgery, Via Alvaro del Portillo 21, 00128, Rome, Italy
[g] University of Bologna, Department of Pharmacy and Biotechnology, via Irnerio 42, 40126, Bologna, Italy
[h] Institute of Nanostructured Materials, National Research Council (ISMN-CNR), Via Piero Gobetti, 101, 40129, Bologna, Italy
[i] IRCSS Istituto Ortopedico Rizzoli, BST Biomedical Science and Technologies Lab, via di Barbiano 1/10 40136, Bologna, Italy
[j] University of Bologna, Department of Biomedical and Neuromotor Sciences, Via Massarenti, 9 40128, Bologna, Italy
[k] Sechenov First Moscow State Medical University, Institute of Pharmacy, Department of Analytical, Physical and Colloid Chemistry, Trubetskaya 8, build. 2, 119991, Moscow, Russia

ARTICLE INFO

Keywords:
Tricalcium phosphate
Silver
Nanostructured coatings
Antibacterial coatings
Orthopedics
Antibacterial ceramics

ABSTRACT

Orthopedic infections pose severe societal and economic burden and interfere with the capability of the implanted devices to integrate in the host bone, thus significantly increasing implants failure rate. To address infection and promote integration, here nanostructured antibacterial and bioactive thin films are proposed, obtained, for the first time, by Ionized Jet Deposition (IJD) of silver-substituted tricalcium phosphate (Ag-TCP) targets on titanium. Coatings morphology, composition and mechanical properties are characterized and proof-of-concept of biocompatibility is shown. Antimicrobial efficacy is investigated against four Gram positive and Gram negative bacterial strains and against *C. albicans* fungus, by investigating the modifications in planktonic bacterial growth in the absence and presence of silver. Then, for all bacterial strains, the capability of the film to inhibit bacterial adhesion is also tested. Results indicate that IJD permits a fine control over films composition and morphology and deposition of films with suitable mechanical properties. Biological studies show a good efficacy against *Escherichia coli, Staphylococcus aureus, Pseudomonas aeruginosa, Enterococcus faecalis* and against fungus *Candida albicans*, with evidences of efficacy against planktonic growth and significant reduction of bacterial cell adhesion. No cytotoxic effects are evidenced for equine adipose tissue derived mesenchymal stem cells (ADMSCs), as no reductions are caused to cells viability and no interference is assessed in cells differentiation towards osteogenic lineage, in the presence of silver. Instead, thanks to nanostructuration and biomimetic composition, tricalcium phosphate (TCP) coatings favor cells viability, also when silver-substituted. These findings show that silver-substituted nanostructured coatings are promising for orthopedic implant applications.

1. Introduction

Healthcare-related infections are among the most diffused and severe complications deriving from the implantation of bone prostheses and medical devices in general (~4 million cases occur per year in Europe, resulting in a burden of ~37.000 deaths and a direct cost of ~7 billion Euros for surgery, therapy and prolonged hospitalization) [1]. Treatment of implant infections is challenging, especially when biofilm forms, and can require implant removal and revision surgeries [2]. The

Peer review under responsibility of KeAi Communications Co., Ltd.
* Corresponding author.
E-mail address: gabriela.graziani2@unibo.it (G. Graziani).

https://doi.org/10.1016/j.bioactmat.2020.12.019
Received 22 October 2020; Received in revised form 10 December 2020; Accepted 20 December 2020
Available online 5 January 2021

progressive development of highly porous and highly rough implants (such as custom-made 3D printed prostheses, nano/micro patterned surfaces, etc.), born to promote implants osseointegration, does negatively impact on infections. In fact, all the features that increase cells adhesion to the substrate and hence, their proliferation and differentiation ultimately leading to bone regeneration, also tend to increase bacterial adhesion, and the cascade of events leading to biofilm formation and infection [3,4]. As a consequence, prevention of infections is a key goal in orthopedics, which can be achieved by a coating able to locally deliver the antibiotic agent in a tuned concentration directly in the infection site [3]. With this aim, metallic coatings, and especially silver coatings, have been widely investigated and used in the clinical practice. Ideal coatings to be applied on bone implant surfaces, however, should not only fight infections, but also promote osseointegration and, hence, bone regeneration [4]. However, promoting integration and even avoiding interference with bone healing might not be trivial, as antibacterial compounds are often toxic also to the bone-cells [5]. Nanostructuration of the coating surface permits a fine tuning of ion-release, favoring the achievement of antibacterial efficacy without causing cytotoxicity [5]. At the same time, thickness at the submicrometric scale permits to avoid mechanical mismatch, which can cause coatings fracturing and detachment, ultimately leading to inflammation.

Abbreviations

TCP	tricalcium phosphate
Ag-TCP	silver-substituted tricalcium phosphate
Ag-TCP-t	silver-substituted tricalcium phosphate target;
CaP	calcium phosphate
IJD	Ionized Jet Deposition
PLD	Pulsed Laser Deposition
PED	Pulsed Electron Deposition
BHI	Brain Heart Infusion
OD_{600}	optical density of the growth medium at 600 nm
ADMSCs	mesenchymal stem cells derived from equine adipose tissue
MSCs	mesenchymal stem cells

To achieve pro-osseoinductive and antibacterial effects at one same time, substituted hydroxyapatite-based coatings have been largely used [6–11]. More recently, a special attention has been devoted to other calcium phosphates having higher solubility and dissolution rate, in particular to tricalcium phosphate (TCP), exhibiting improved performances [12–16] and a more sustained silver release. For this reason, Ag substituted TCP (Ag-TCP) was studied in different forms and mainly as moldable, injectable cements [17,18]. However, TCP deposition by a plasma assisted technique, to achieve the formation of nanostructured thin films, is challenging. In fact, multiple requirement must be met for a coating to show suitable performances, such as: (i) absence of cracks, delamination and defects, (ii) a nanostructured surface morphology having high surface roughness, (iii) a submicrometric thickness, to avoid mechanical mismatch with the substrate and to boost adhesion, (iv) high reproducibility in terms of thickness and surface morphology (within one sample and among different samples), (v) absence of formation of potentially toxic byproducts, and a (vi) composition as similar as possible to that of the material to be deposited (target) [19–21]. However, among currently available plasma-assisted techniques, deposition by plasma spray generally lacks homogeneity in composition, thickness and surface morphology and produces thick films (50–200 μm) that tend to undergo fracturing and delamination. In addition, decomposition phases might be formed, such as cytotoxic calcium oxide, that has been frequently detected upon deposition of calcium phosphates. Coatings obtained by magnetron sputtering show a more promising behavior, but still their composition might be different from that of the deposition target, due to preferential sputtering of calcium and/or to evaporation of P_2O_5. In addition, pre- or post-deposition treatments are normally necessary to guarantee suitable adhesion to the substrate [22]. For this reason, nanostructured TCP thin films have been scarcely explored in the literature, especially for what regards ion-substituted TCP [19,23–30].

To obtain Ag-TCP coatings, different methods have been proposed by different research groups, over the last years. However, coatings having features at the nanoscale have been so far only proposed by Socol et al. [18], that applied Combinatorial Pulsed Laser Deposition (PLD) method for Ag-TCP deposition from two separate targets, namely metallic Ag and TCP. The obtained films, deposited on glass slides, were characterized by a linear gradient of Ag content, ranging from 0.94 at% to 0.16 at%. The viability of mesenchymal stem cells was tested. Ag concentration up to 0.6 at% was considered not cytotoxic, although a high solubility of Ag-TCP influenced surface morphology with a drastic reduction of cell adhesion. Coating having micrometric thickness, porosity and surface features have also been proposed by Roy et al. [31], which performed Ag-TCP deposition on titanium (Ti) by means of Laser Engineered Net Shaping. Deposition consisted in two steps: TCP was deposited on Ti, which was successively covered by a film of silver. The obtained films were characterized by different Ag concentrations. *In vitro* antibacterial studies were conducted against *Pseudomonas aeruginosa (P. aeruginosa)* and *Staphylococcus aureus (S. aureus)*. The highest silver concentration (0.5 M) showed the best inhibitory effect in long term use, but was cytotoxic. Therefore, authors recommended formulations at 0.1 M concentration, as they showed good antimicrobial activity and a lower effect on the proliferation of osteoblast precursors. Song et al. [32] proposed micro-arc oxidation technique to deposit Ag-TCP films on Ti substrate. This method allows to deposit films in a wet environment starting from precursors in solution. Biological tests were conducted to evaluate the antibacterial activity against *S. aureus* and *Escherichia coli (E. coli)* and cell viability (MG63 and human osteosarcoma-HOS cells). The authors concluded that all the deposited Ag-TCP films showed very good results as antimicrobial agents independently from the Ag content. No cytotoxicity was observed for the Ag-TCP coatings at the lowest concentration of Ag.

In this work, nanostructured coatings composed of ion-substituted TCP are deposited for the first time by Ionized Jet Deposition (IJD). IJD is selected as it was demonstrated to preserve the stoichiometry from the target to the coatings, even in the case of complex materials, such as biogenic hydroxyapatite, strontium-substituted hydroxyapatite and bioactive glasses [33–35]. In addition, IJD allows achieving a nanostructured surface, promoting host cells adhesion, proliferation and differentiation [36] and providing high specific surface to guarantee a sustained release of the antibacterial agent [37]. Silver-substituted β-TCP is chosen to achieve antibacterial and bioactive efficacy at one same time. The coatings are obtained in one step, by deposition of the Ag-TCP target, without pre- or post-deposition treatments.

The research is devoted to the aims of: (i) demonstrating feasibility of deposition of Ag-TCP nanostructured films by the IJD; (ii) characterizing the obtained films, (iii) obtaining antibacterial efficacy against gram+ and gram-strains, with specific reference to the reduction of bacterial adhesion; (iv) showing the absence of cytotoxicity. The capability of the technique to manufacture ion-substituted metastable calcium phosphates (CaP) coatings is studied, by assessing its fidelity in preserving the composition of the target in terms of: (i) the main CaP phase, TCP and (ii) the presence of silver in the coatings. Then, the coatings are characterized and the antibacterial efficacy and the absence of cytotoxicity are demonstrated, for application in orthopedic prostheses.

2. Materials and methods

2.1. Materials

Ag-TCP (Ag 0.11 mass%) targets (Ag-TCP-t) are prepared as described in the following. The Ag-TCP powder is obtained using mechanochemical activation processing. Reagents are dry-milled for 20 min in a planetary mill with corundum balls in Teflon vessels (material: balls ratio of 1:3), rotation speed being set at 200 rpm. After that, an appropriate quantity of water is added, and another milling cycle is carried out for 20 min. The resulting suspension is filtered and dried at room temperature under dark conditions. During the synthesis process, 0.014 mol of silver nitrate is introduced, so that silver content in the TCP is adjusted to 0.49 wt %, in accordance to the formula reported below. The formation of Ag-TCP is obtained according to the following scheme (1,2):

$$2{,}993CaO+0{,}014AgNO_3+2(NH_4)_2HPO_4 + H_2O \rightarrow Ca_{2,993}Ag_{0,014}(PO_4)_2 + 0{,}014NH_4NO_3 + 3{,}86NH_4OH \quad (1)$$

$$3CaO + 2(NH_4)_2HPO_4 + H_2O \rightarrow Ca_3(PO_4)_2 + 4NH_4OH \quad (2)$$

Chemical elemental analysis is performed using an optical emission spectrometer with inductively coupled plasma (Optima 5300 DV). The silver content, according to elemental analysis, is found to be 0.11 ± 0.05 mass%. The difference between the detected final silver content of 0.11 mass% and that theoretically calculated by the formula $Ca_{2,\ 993}Ag_{0,\ 014}(PO_4)_2$ (0.49 mass%) is due to the fact that, during the synthesis process, part of the silver ions interact with ammonium ions to form a water-soluble silver ammonia complex, according to the reaction:

$$Ag^+ + 2NH_3 \rightarrow [Ag(NH_3)_2]^+ \quad (3)$$

Green ceramics target samples are obtained by uniaxial pressing in a steel mold at 300 MPa. The ceramic discs are then sintered at 1300 °C for 2 h.

Medical grade titanium alloy disks (Grade 23 Titanium 6Al-4V ELI alloy, 5 mm of thickness, 5/10 mm of diameter, Citieffe S.r.l.) are used as substrates for the deposition, after ultrasonic cleaning in isopropyl alcohol and water. A surface roughness (Ra) of 5 μm is specifically selected as representative of that of orthopedic implants. Silicon wafers (Si) (p-type doped monocrystalline (100) native silicon, size 5 × 5 mm, thickness 1 mm, Fondazione Bruno Kessler, Trento, Italy) are also used as reference substrate for the morphological and compositional characterizations. All mechanical and biological tests are carried out on titanium alloy disks, as they are more representative of orthopedic implants. No surface preparation in terms of polishing, machining, etching or surface patterning is carried out prior to deposition, for any of the substrates.

2.2. Methods

2.2.1. Targets characterization

Targets are characterized by X-ray diffractometry (XRD - Shimadzu 6000 diffractometer, CuK_α radiation) in the range of 20–80° (2θ), Scanning Electron Microscope (SEM - EVO/MA10, ZEISS, equipped with an Energy Dispersive X-ray Spectrometry system - EDS, INCA Energy 200, Oxford Instruments, UK) and Attenuated Total Reflection Fourier-transform infrared spectroscopy (FT-IR/ATR) (PerkinElmer Spectrum 2, USA), to verify the compliance to the expected composition.

2.2.2. IJD deposition

Ag-TCP coatings are realized by Pulsed Electron Deposition in the Ionized Jet Deposition (IJD) setup (Noivion Srl, IT). For the deposition, the Ag-TCP target (Ag-TCP-t) is mounted on a rotating target holder and ablated by a fast pulse (100 ns) of high energy (10 J) electrons and high-density power. To ensure uniformity in deposition, the substrate is kept rotating during the whole process and first 5 min of deposition are performed on a shutter. Target-substrate distance is optimized and adjusted to 8 cm, based on uniformity of deposition (data not shown). The vacuum chamber is initially evacuated down to a base pressure of 1.0×10^{-7} mbar by a turbomolecular pump (EXT255H, Edwards, Crawley, UK) and then raised by a controlled flow of oxygen (purity level = 99.999%) up to 3×10^{-4} mbar. Prior to deposition, the surface of the target is cleaned by setting the electron beam at 8 kV and 7Hz for 15 min, to remove possible surface impurities. Then, for deposition, the working voltage and the electron beam frequency are set at 17 kV and 7 Hz, respectively. The parameters used in this work have been selected based on the preliminary studies regarding CaP film growth at different acceleration voltages, frequencies and target-to-substrate distances.

Deposition times of 10, 20 and 30 min, being the highest deposition time that can be achieved by the deposition of one same target, are tested. Based on the deposition time, coatings deposited onto the Ti alloy plates are referred to as Ag-TCP-10, Ag-TCP-20, Ag-TCP-30, where the last number represents the duration of deposition. To discriminate among samples deposited on Si wafers and Ti alloy plates, samples deposited onto the wafers are referred to as Si- followed by deposition time in minutes (e.g. Si-10, Si-20, Si-30).

2.2.3. Film characterization and selection of the most promising coating

First, coatings uniformity and surface texture depending on deposition times are evaluated by SEM, to select those having the highest uniformity and to discard those exhibiting insufficient substrate coverage and/or cracking due to excessive thickness.

Coatings morphology is analyzed by Field Emission Gun Scanning Electron Microscopy (FEG-SEM, Tescan Mira3, CZ, working distance = 10 mm, voltage = 10 kV), on both the Ti and Si substrates. FEG-SEM samples were made conductive by sputtering with aluminum before observation. Based on FEG-SEM images at 50.000× magnification, the dimension of the aggregates that constitute the films was measured by ImageJ software (National Institutes of Health, USA). To analyze the distribution in aggregates diameters, 3 non overlapping areas of two samples were selected, each composed by at least 45 clearly distinguishable aggregates. All areas had the same dimensions and were chosen within images at a 50.000× magnification. Maximum, minimum and average diameter (d) were calculated for each area and sample, and then averaged. Distribution was studied by dividing the aggregates in four groups, selected based on the maximum, minimum and most frequent diameters: $d < 50$ nm, $50\ nm \leq d < 100$ nm, $100\ nm \leq d < 500$ nm, $d \geq 500$ nm. The percentage of aggregates having diameters within each range was calculated.

Samples topography was also investigated on Si wafers by Atomic Force Microscopy (AFM) using a Multimode VIII equipped with a Nanoscope V controller, Bruker, USA). The AFM was operated in the ScanAsyst Imaging mode using NT-MDT cantilever NSG10 with a nominal spring constant of 3.1 N/m. Based on AFM images, the surface roughness was calculated as RMS by Gwyddion after performing a plane subtraction 0 order line-flattening [38].

Film thickness was measured by SEM on Si and Ti substrates, by scratching the coating surface and tilting it for acquisition. Thickness measurements were obtained as average of 4 measures carried out into non-overlapping areas in 2 samples. Surface roughness was measured.

Films composition is evaluated by Energy Dispersive X-ray Spectroscopy (EDS) and FT-IR/ATR on samples deposited onto Ti substrates and Si wafers, respectively. For the EDS, 3 non-overlapping regions of two different samples were examined. The EDS analysis was performed using a Bruker probe coupled with a field emission gun scanning electron microscope (FEG-SEM, Tescan Mira3). A working voltage of 10 kV was used. The samples were made conductive before observation by coating with aluminum.

FT-IR spectra (PerkinElmer Spectrum 2) are collected in the Attenuated Total Reflection (ATR) mode, using a diamond crystal, a resolution of 4 cm^{-1}, a scan step of 0.5 cm^{-1} and 32 accumulations.

Based on the reported characterizations, the most promising condition (corresponding to the Ag-TCP-30 sample) was selected, and the sample was characterized from mechanical and biological point of view, to investigate its suitability for the proposed goal. All the samples were deposited on the Ti alloy plates to mimic deposition onto orthopedic implants.

2.2.4. Mechanical tests

Vickers microhardness mechanical test on the films is performed for coatings deposited for 30 min on Ti plates (Ag-TCP-30) by means of a Leica VMHT apparatus (Leica GmbH, Germany), equipped with a standard Vickers pyramidal indenter (136° face angle square-based diamond pyramid). Five loads, ranging from 0.049 up to 0.49 N, are applied at 15 s of the loading and unloading speed of 5×10^{-6} m/s. Ten indentations are made at each load. Measurements and data analyses are performed according to a procedure described in detail in the previous work [39]. Hardness of the Ti substrate measured in a separate experiment is equal to 2.0 ± 0.2 GPa. For the deposited coatings, the measured hardness is that of the film/substrate composite system.

2.2.5. Stability of the coating in physiological-like environment

Stability of sample Ag-TCP-30 was evaluated by immersion in sterile alpha-MEM (Minimum Essential Medium Eagle, Sigma Aldrich) for 24h, 7 days, 14 days and 20 days, respectively. The medium was supplemented with 1 wt% penicillin-streptomycin to avoid bacterial contamination and pH was adjusted to 7.4 by addition of $NaHCO_3$ (2.2 g/l). Films were placed in 24 wells and 1 ml medium was put into each well. Wells plates were sealed and kept in a humidified incubator at 37 °C, 95% air and 5% CO_2. Medium was refreshed every 72h.

Stability was evaluated by examining coatings morphology by the SEM/EDS after immersion at each timepoint. The SEM/EDS was performed as described in §2.2.3 on at least 2 non-overlapping areas of each sample, 1 close to the center and 1 on the samples edge. Specific attention was devoted to the coating integrity at each timepoint and to the presence/absence of cracks and detachments, which could cause inflammation and toxicity *in vivo*.

2.2.6. Antimicrobial tests

Inhibition of microbial planktonic growth

The antimicrobial activity of Ag-TCP against the planktonic growth of pathogenic strains belonging to *E. coli, Enterococcus faecalis (E. faecalis), P. aeruginosa, S. aureus* bacteria, and *Candida albicans (C. albicans)* fungus was assessed. Antimicrobial tests were carried out on the coated Ti substrates. For Ag-substituted TCP, the test was carried out on the most promising coating (deposition time 30 min), selected based on morphological and compositional characterizations.

The study was carried out by growing the microorganisms in Brain Heart Infusion (BHI, DIFCO, concentration 37 g in 1 L sterile distilled water) alone and in the presence of TCP and Ag-TCP (1 cm diameter disks) for 24 h. Prior to the tests, TCP and Ag-TCP samples were autoclaved at 121 °C for 20 min at pressure of 1.1 bar. The four bacterial strains and the fungus were first grown in BHI overnight at 37 °C and 30 °C, respectively, under agitation at 150 rpm. For the tests, all the bacteria and *C. albicans* were diluted to reach $OD_{600} = 0.1$. TCP and Ag-TCP were immediately inserted into 2 mL solution after diluting. At the end of the incubation, the growth of the various microorganisms was assessed by measuring the optical density of the growth medium at 600 nm by BioPhotometer (Eppendorf, Germany). Each experiment was repeated in triplicate.

Inhibition of bacterial cells adhesion

The anti-adhesion property of Ag-TCP was determined for the four bacterial pathogens *E. coli, E. faecalis, P. aeruginosa,* and *S. aureus*. As for the determination of inhibition of microbial planktonic growth, the tests were carried out on the coated Ti plates (Ag-TCP-30). The bacteria were grown overnight in BHI at 37 °C with aeration at 150 rpm. The bacterial cell suspensions were diluted to reach $OD_{600} = 0.2$. Sterile TCP and Ag-TCP coated Ti plates were transferred into 1 mL bacterial suspensions placed in 24-well microplates. To allow adhesion, microplates were incubated for 4 h at 37 °C with gentle shaking (50 rpm). The TCP and Ag-TCP were removed from the cultures and rinsed twice with 0.85% NaCl (w/v) to wash away the non-attached cells. The adherent cells were first fixed with 99% ethanol (v/v) for 10 min and then stained with 0.2% crystal violet (w/v) with an incubation time of 10 min at room temperature. The excess of unbound crystal violet was removed by washing the TCP and Ag-TCP three times with sterile water. The bound dye was extracted with 33% acetic acid (v/v). The amount of cell adhesion was measured at optical density of 595 nm. The background staining was corrected by subtracting the mean value for crystal violet bound to negative controls. Each experiment was repeated in triplicate.

2.2.7. Cytotoxicity and bioactivity

Isolation and culture of mesenchymal stem cells derived from equine adipose tissue (ADMSCs).

Cytotoxicity (MTT Test) and differentiation studies in the osteogenic lineage in the presence of TCP- and Ag-TCP- coated Ti plates were carried out on ADMSCs. ADMSCs are selected as they are frequently used as stem cell source for bone tissue repair, due to their high availability, high potential for differentiation and the possibility to be extracted by means of minimally invasive techniques. Subcutaneous adipose tissue was taken from a 2 years old male slaughtered horse and quickly transported refrigerated to the laboratory. The tissue was washed 3 times with saline phosphate buffer (PBS, from Sigma-Aldrich) supplemented with 5% v/v penicillin-streptomycin (Sigma-Aldrich) under sterile conditions. Subsequently, it was cut into small pieces, digested at 37 °C for 1 h under stirring with 0.1% of collagenase IA (Sigma-Aldrich) and centrifuged at 800g for 10 min. The obtained cell pellet was resuspended in Dulbecco's modified Eagle growth medium (DMEM, Gibco) with 10% (v/v) fetal bovine serum (FBS, Gibco), cultured in cell culture flask (Falcon) and incubated at 37 °C with 5% CO_2 in a humidified atmosphere. After 24 h, the growth medium was changed to remove cellular debris. This procedure was repeated every two days until the confluence of 80–90% of the cell monolayer was reached.

2.3. Study of the effect of Ag-TCP on cell viability - MTT test

Cells viability on Ag-TCP and TCP coated Ti plates was measured indirectly, based on the MTT colorimetric test. The MTT evaluates the enzymatic reduction by mitochondrial succinate dehydrogenase (SDH) of 3- [4,5-dimethylthiazole-2-yl] −2,5-diphenyltetrazolium bromide (MTT, Sigma-Aldrich) in salts of blue formazan (insoluble in water). As a consequence, the quantity of the produced formazan is proportional to the presence of viable cells. In this experiment, the ADMSC monolayer at 80–90% confluence was trypsinized (Sigma-Aldrich trypsin). Cells were resuspended at a concentration of 40,000 cells/mL in growth medium (DMEM integrated with 10% FBS), distributed in 24-well plates and incubated at 37 °C at 5% CO_2. 1 ml medium was added in each well, so the resulting cells density was 40.000 cells per well. After 24 h, the samples of TCP and Ag-TCP (autoclaved before use at 121 °C for 20 min at pressure of 1.1 bar) were placed on the ADMSC monolayer and incubated for another 24 h under the same conditions. At the end of the incubation, the growth medium was replaced by the MTT diluted in DMEM (0.5 mg/mL). After 3 h of incubation at 37 °C, the MTT solution was replaced with isopropanol (Sigma-Aldrich) and kept at room temperature for 30 min. During this incubation, the produced formazan was solubilized and measured at the OD of 600 nm by a BioPhotometer. To measure viability, all data were expressed as a percentage to the OD of the control (cells cultured on plastic multi-wells). All the experiments were carried out in triplicate.

2.4. Effect of Ag-TPC on osteogenic differentiation

Possible impairment of cells differentiation in the presence of TCP and Ag-TCP coated Ti plates was qualitatively investigated. To this aim, the ADMSC were diluted in growth medium at a concentration of 40,000 cells/ml, then placed in a 6-well plate (Falcon) and incubated at 37 °C in CO_2. 3 ml medium were put into each well, hence a density of 60.000 cells/well was reached. After 24 h of incubation, the growth medium was replaced with an osteogenic medium formed by DMEM with the addition of 10% FBS, ascorbic acid 50 μg/mL (Sigma-Aldrich), β-glycerophosphate 10 mM (Sigma-Aldrich) and dexamethasone 10^{-7} M (Sigma-Aldrich). The ADMSCs were incubated at 37 °C and 5% CO_2 for three weeks, changing the growth medium and osteogenic medium every two days. Negative control was obtained by growing the ADMSCs in the growth medium, while positive control was obtained by growing the ADMSCs in the osteogenic medium. Osteogenic differentiation was highlighted by staining with Alizarin Red S (Sigma-Aldrich), which marks calcium present in the extracellular matrix in red. The observation of the cell monolayer was carried out by an inverted optical microscope (Nikon, Eclipse, JP).

2.4.1. Statistical analyses

All the results are reported as mean ± standard deviation (SD) calculated from three replicates. Statistical analysis was performed using one-way Anova test. Differences were considered significant for $P < 0.05$.

3. Results and discussion

The XRD spectrum of the Ag-TCP target is presented in Fig. 1. A spectrum of pure TCP has been reported in the supplementary material, Fig. S1, for comparison sake.

In Fig. 1b, theoretical and experimental values of Bragg reflection positions for Ag-TCP targets are reported, extrapolated from literature data (β-TCP, PCPDF #70-2065) and from the experimental diffraction pattern, respectively. The last column of Fig. 1b shows calculated position shifts (Δ 2θ). Almost all experimental 2θ positions present negative shift, meaning that the Bragg reflections are characterized by a deviation towards lower angles, causing increased distances between lattice planes. This result is consistent with experimental evidences reported in the work of other authors [40,41] and is a well-known phenomenon that occurs when calcium phosphate lattice accommodates foreign cations or anions in a specific lattice site. A common interpretation relies on the comparison of ionic radii of atomic species which compete for the same site. In our case, the larger Ag ionic radius (115 p.m.) compared with Ca ionic radius (99 p.m.) implies a slight distortion of TCP lattice with a sensible increase of lattice parameters and interplanar distances.

Morphology of the uncoated Ti substrate is shown in the supplementary material in Fig. S2, coatings surface morphology is shown in Fig. 2 and Fig. 3. The aggregates are uniformly distributed on the substrates and no defects, such as uncoated areas and/or cracks detachments, are noticed for any of the deposition times. Maximum and minimum diameters of the aggregates are reported in Table 1. Deposition on Si wafers (Fig. 2, Table 1) shows that the films are composed of globular aggregates, whose diameter spans from 20 nm to 1100 nm, for deposition times of 10 and 30 min, respectively. Interestingly, 20 min deposition results into a higher variability and in the formation of isolate clusters of bigger dimensions (Fig. 2), that reach diameters close to 2 μm. The presence of these big clusters becomes negligible for increasing deposition times, as the coating grows over the underlying layers of aggregates, progressively flattening irregularities, as already reported for zirconia thin films deposited by Pulsed Electron Deposition (PED) [42]. In general, however, the increase in deposition time results into the progressive formation of more diffused and larger clusters of globular aggregates, as can be noticed in Fig. 2 c, f, i and in Table 1, where a progressive decrease in the amount of aggregates in the finer fraction ($d < 50$ nm) and an increase in the coarser fraction ($d \geq 500$ nm) are noticed for increasing time. This behavior is characteristic of PED and IJD, and has been reported for different ceramic and ceramic-like materials, including bone apatite and bioactive glasses [33,35].

For Si, thickness of 163 ± 69 nm, 207 ± 74 nm and 188 ± 30 nm is measured for deposition times of 10, 20 and 30 min, respectively. Hence, while thickness increases for deposition times up to 20 min, switching from 20 to 30 min does not result in coarser films, but into lower heterogeneity. These data confirm what seen for the formation of clusters, i.e., as the deposition proceeds, the aggregates tend to concentrate in the valleys formed among them rather than on top of one another, progressively flattening the depth profile.

When applied to Ti substrates (Fig. 3), the coatings do not alter their micro-scale surface finishing, which is important for application in orthopedic implants, as it is specifically designed by the manufacturers to guarantee primary stability (Fig. 3 a,b,d,e,d,h). For Ti substrates, deposition times up to 30 min are permitted, without experiencing cracking and detachments, as in the case of Si wafers.

Aggregates show diameters ranging from ≈10 nm to ≈1 μm (Table 1). Coatings at 10 min deposition time show relevantly finer aggregates and the formation of clusters of smaller dimensions. As for Si substrates, no significant differences are assessed in maximum and minimum diameter between 20 and 30 min of deposition. Again, the increase in deposition time results into a progressive decrease in the amount of aggregates in the finer fraction ($d < 50$ nm) and an increase in the coarser fractions ($100 \text{ nm} \leq d < 500$ nm), as well as in the average diameter.

a)

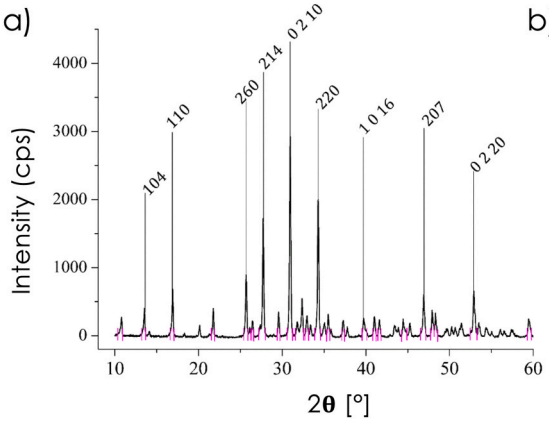

b)

Peak (hkl Miller Index)	Relative Intensity (%)	Theoretical 2θ (°)	Experimental 2θ (°)	Shift (Δ 2θ)
0 1 2	15	10.863	10.8	-0.063
1 0 4	21	13.618	13.54	-0.078
1 1 0	25	16.974	16.92	-0.054
0 2 4	13.5	21.825	21.76	-0.065
1 0 10	26	25.773	25.68	-0.093
2 1 4	56	27.78	27.72	-0.06
3 0 0	13	29.62	29.56	-0.06
0 2 10	100	31.02	30.96	-0.06
2 2 0	70	34.33	34.3	-0.03
1 0 16	10	39.83	39.74	-0.09
4 0 10	22	46.94	46.9	-0.04
2 0 10	25	52.9	52.98	+0.08
2 4 10	7.5	59.44	59.46	+0.02

Fig. 1. a) X-ray diffraction spectrum of Ag-TCP powder. The peaks were assigned using Reference card number of β-TCP n° PCPDF #70-2065. b) Ag-TCP X-ray powder diffraction data (Relative Intensity (%) theor.).

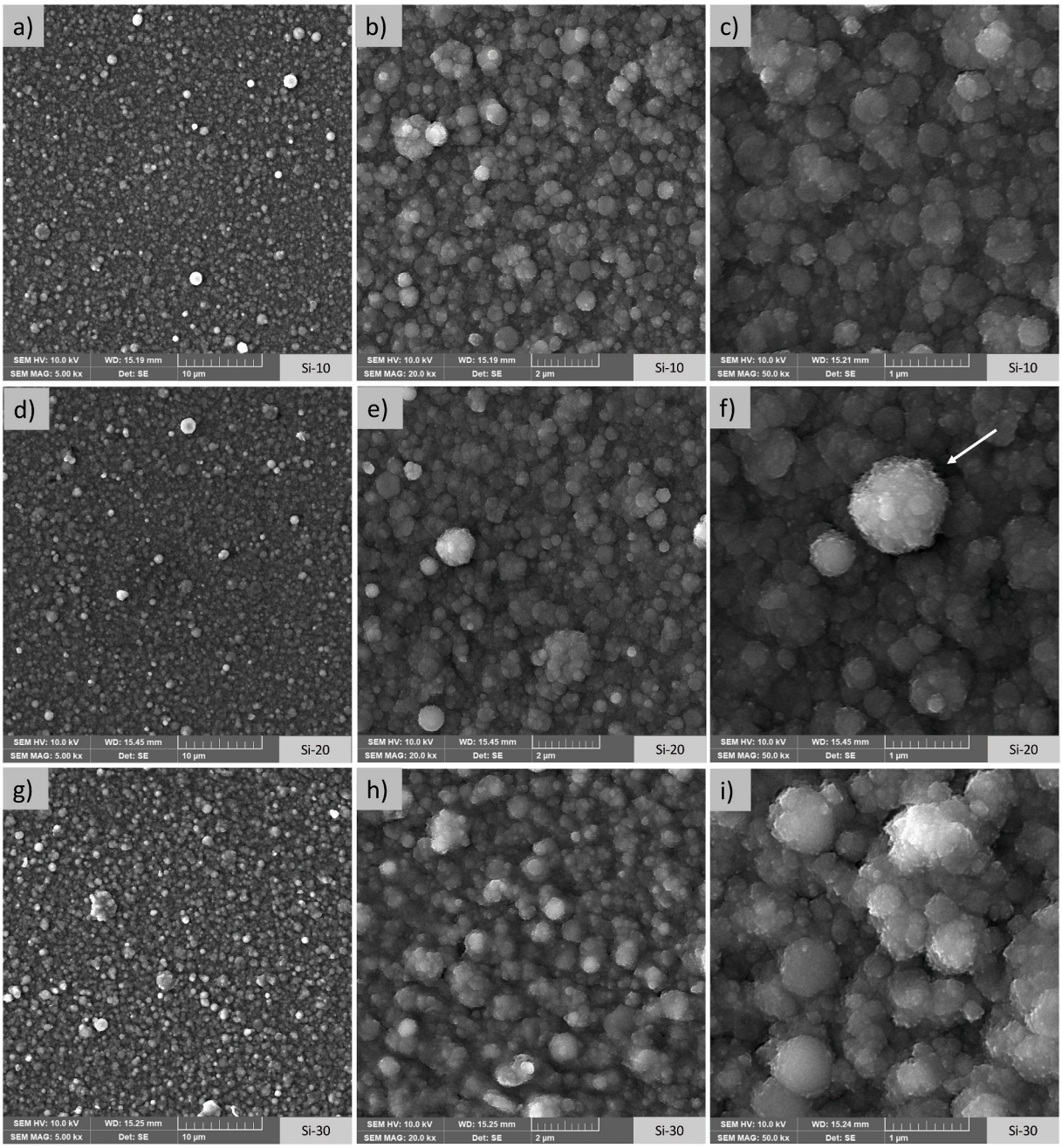

Fig. 2. Surface morphology of the thin films on Si wafers after 10 min (a,b,c), 20 min (d,e,f) and 30 min (g,h,i) of deposition. Images at 5000× magnification (a,d,g) show a high uniformity in the substrate coating without formation of cracks. At higher magnification (20.000x-b,e,h and 50.000x-c,f,i) Si-20 and, mostly, Si-30 show a more abundant presence of bigger clusters. In (f), sparse aggregates of bigger size are noticed on the sample Si-20 (shown by an arrow).

Comparing growth on Si and Ti substrates, it is clear that all films, negligent of substrate and deposition time are nanostructured, as they are composed by nanosized globular aggregates, but surface morphology is strongly determined by the deposition time. For increasing deposition times, up to 20 min, for both the Si and Ti substrates, the spheres that constitute the coatings tend to aggregate in larger clusters, increasing surface roughness and leading to a higher dispersion in the diameter of the globules. This effect is slightly more visible for the Ti substrate, although no significant differences are found between the two. From 20 to 30 min depositions, instead, the dimensions of the aggregates remain substantially unaltered, while heterogeneity decreases for Si. For Ti, where no significant heterogeneity is found at 20 min, cluster size continues to increase. In addition, when compared to Ti, deposition onto Si results in the formation of bigger aggregates and clusters, indicating a non-negligible influence of the substrate composition and topography on coatings characteristics and a higher homogeneity for deposition onto rough substrates.

RMS calculations and AFM images are shown in Fig. 4. Values of RMS of 52 ± 6 nm, 69 ± 27 nm and 78 ± 16 nm are measured for deposition times of 10, 20 and 30 min. A high roughness is found for all the samples, which increases for increasing the deposition time. In addition, the AFM acquisitions at 20 min indicate the presence of isolate aggregates of bigger diameter (Fig. 4e), which are not observed for the other conditions, as already assessed by SEM. The presence of these aggregates significantly impacts on the roughness variability within the sample, as demonstrated by the high standard deviation in the graph (Fig. 4a).

The beneficial effect of nano- and micro-sized topographical cues and, in particular, of nanoscale topography and nanoroughness on cells

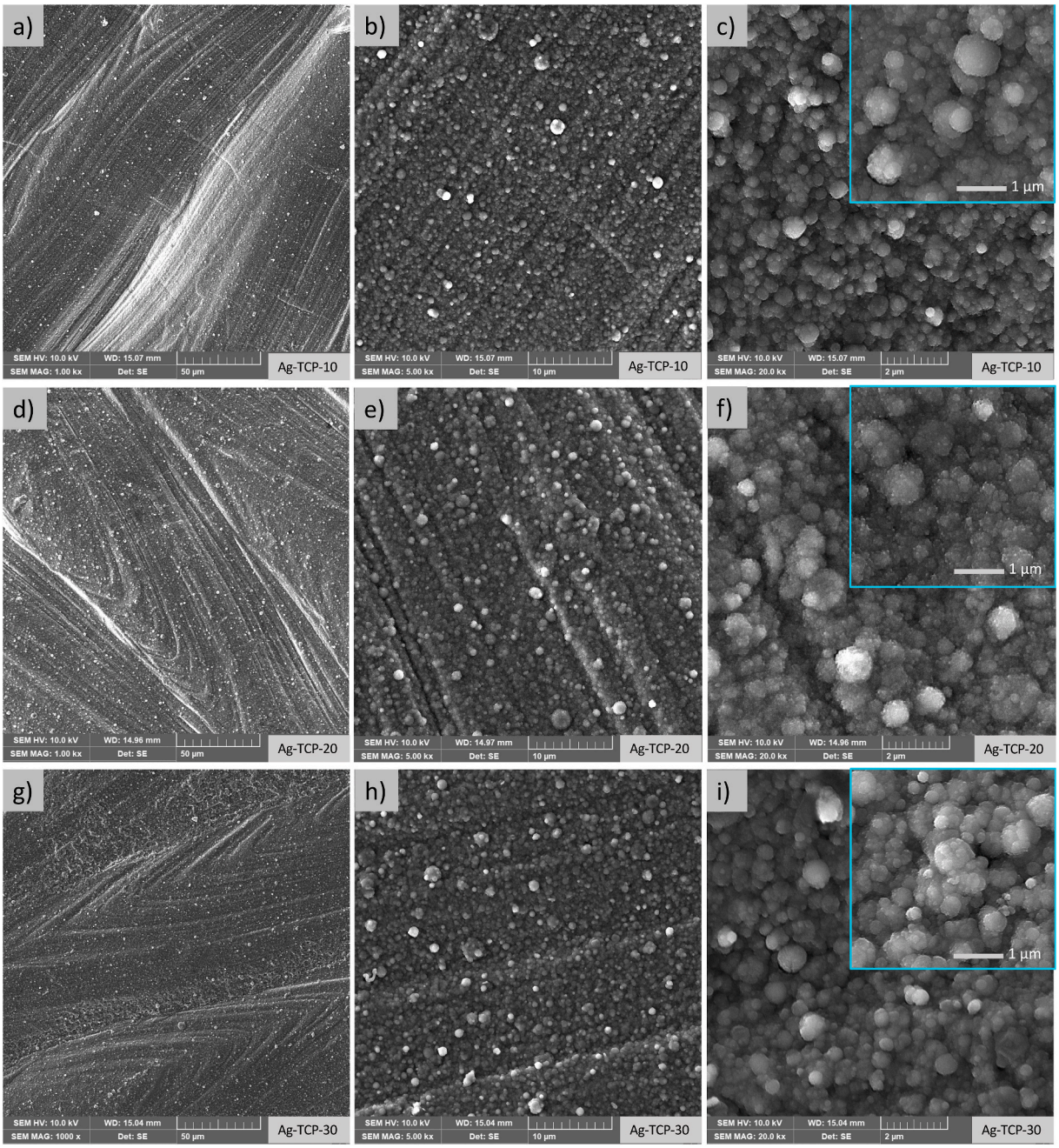

Fig. 3. Surface morphology of the thin films on Ti alloy disks after 10 min (a,b,c) and 30 min (d,e,f) deposition. Images at 1.000× and 5.000× magnification (a,b,d,e) show that surface features at the micro- and macro-scale are preserved.

Table 1
Dimensional distribution of the aggregates in the thin films deposited onto Si (Si-10, Si-20, Si-30) and Ti substrates (Ag-TCP-10, Ag-TCP-20, Ag-TCP-30).

	Dmax	Dmin	Mean D	Distribution [%aggregates for each range]			
	[nm]	[nm]	[nm]	d < 50 nm	50 nm ≤ d < 100 nm	100 nm ≤ d < 500 nm	d ≥ 500 nm
Si-10	1095	16	132	44 ± 2	28 ± 5	24 ± 8	4 ± 2
Si-20	1787	20	237	14 ± 1	44 ± 14	34 ± 13	8 ± 3
Si-30	1131	17	198	26 ± 5	18 ± 6	44 ± 6	12 ± 5
Ag-TCP-10	830	11	153	53 ± 3	14 ± 5	28 ± 2	6 ± 2
Ag-TCP-20	959	22	167	28 ± 3	33 ± 1	32 ± 3	7 ± 3
Ag-TCP 30	927	22	178	23 ± 5	18 ± 5	53 ± 13	6 ± 1

adhesion, proliferation and on MSCs differentiation has been demonstrated and is an object of increasing attention [43–46], hence confirming that micro/nano features are recommended for bone implants [47,48]. As a consequence, surface nanostructuration by TCP and Ag-TCP coatings is expected to contribute in favoring host cells viability and mitigating possible toxic effects of silver. In addition, thanks to the

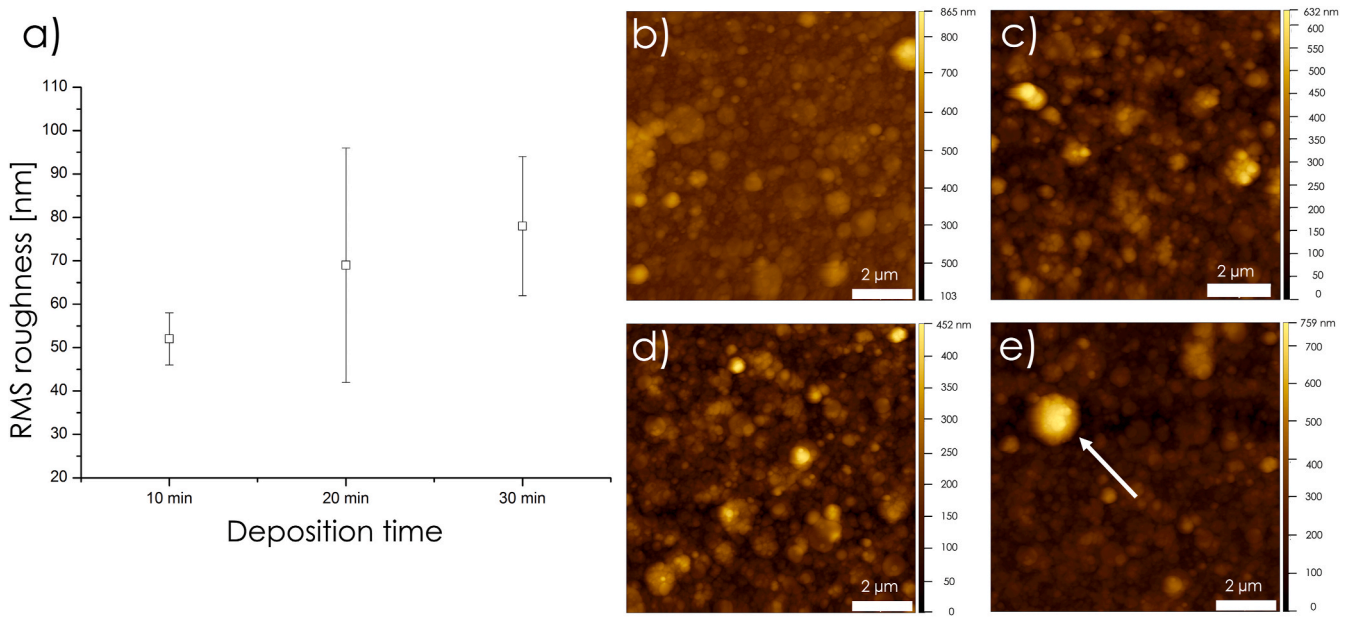

Fig. 4. Roughness (a) and AFM images (b–e) of samples, depending on deposition time. Images (b) and (c) show surface topography of samples deposited for 10 and 30 min (Si-10 and Si-30), respectively. In (d) and (e), the topography of Si-20 is shown; the arrow in Figure (e) indicates the larger clusters already observed by the FEG-SEM, determining high variability in the sample roughness.

high specific surface area, the release of silver is facilitated, which is expected to increase antimicrobial efficacy.

Here, a higher surface uniformity is found for increasing deposition time, from 20 to 30 min, as the aggregates become more regular and show a better dispersion in size distribution from the nano-to the micro-scale (Table 1). As a consequence, deposition time of 30 min shall be preferred. For the selected conditions, film thickness on Ti corresponds to 301 ± 45 nm.

FT-IR graphs of Ag-TCP coating (Si-30, Fig. 5a) show bands at 1117 cm^{-1} (ν_3HPO_4 or combination), 1043 cm^{-1} (ν_3PO_4 antisymmetric stretch), 1015 cm^{-1} (ν_3PO_4 antisymmetric stretch, also compatible with carbonated hydroxyapatite), 970, 945 cm^{-1} (ν_1PO_4 symmetric stretch), 608, 546 cm^{-1} (ν_4PO_4 antisymmetric bend). All these bands correspond to those found in the Ag-TCP target, indicating an effective transfer of target composition during deposition. No deposition phases or bands relative to other CaPs are detected. Band at 730 cm^{-1} is relative to the substrate. In addition, bands are visible at 1451, 1410 (asymmetrical and symmetrical stretching modes of $CO_3\nu_3$) and 871 cm^{-1} (ν_2CO_3), all characteristics of carbonates. These bands, together with the shift in the band at 1015 cm^{-1}, indicate the formation of carbonated hydroxyapatite (CHA) as a consequence of the deposition process. CHA has been already reported for deposition of calcium phosphates by IJD [33,36,49] with no detrimental effects, consistently with it being the main phase in biogenic apatite.

FT-IR spectra of samples deposited at 10, 20 and 30 min are reported in the supplementary material, Fig. S3. Due to the reduced thickness of the films, decreasing the contribution of the coating signal compared to that of the substrate (for sample Ag-TCP-10) and to the high heterogeneity reducing the area of contact between the coating and the detector (Ag-TCP-20), both making the contact with the detector imperfect and reducing the overall intensity of the signal, curves of Ag-TCP-10 and Ag-TCP-20 appear broad and ill-defined. As a consequence, a precise attribution of the bands cannot be performed. However, the presence of bands at 1000-1100, 600 and 560 cm^{-1} confirms deposition of a calcium

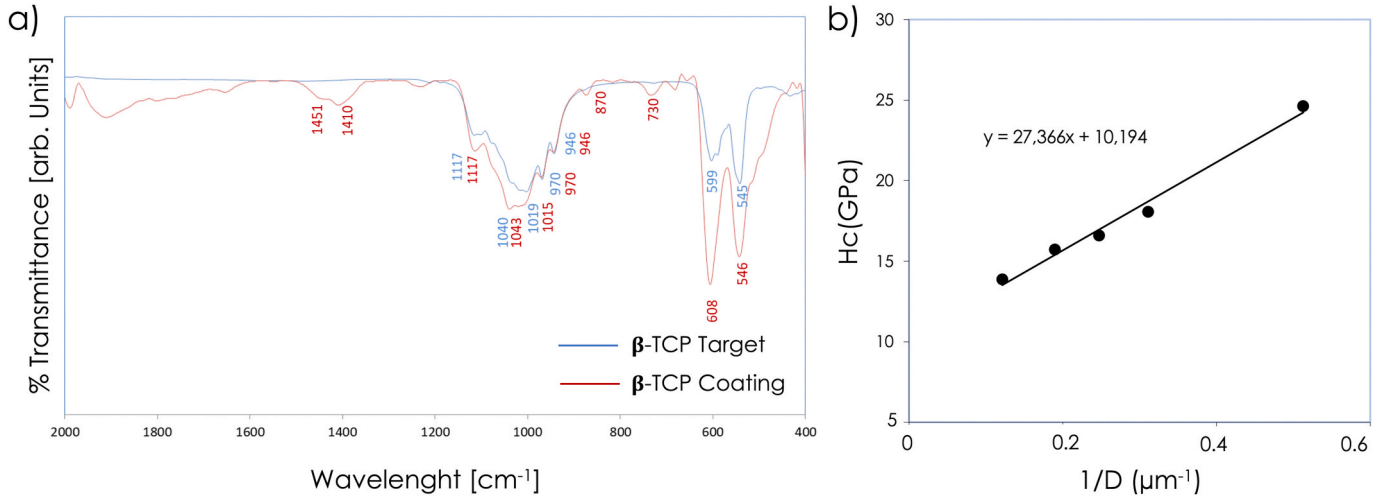

Fig. 5. Characterization of the deposited coatings: a) FT-IR/ATR spectra of coatings and targets; b) composite film-substrate hardness plotted versus the inverse imprint diagonal.

phosphates-coating. The higher intensity of the substrate band at 730 cm^{-1} in Si-10 confirms the lower thickness of the film.

EDS spectra indicate the presence of Ag in all the deposited films, in a concentration lower than the nominal concentration in the target (0.15 wt%), the average being 0.07 ± 0.05 wt% for Ag-TCP-10, 0.10 ± 0.095 wt% for Ag-TCP-20 and 0.08 ± 0.03 wt% for Ag-TCP-30. This experimental evidence is not surprising, since IJD capability to preserve target stoichiometry can depend on the characteristics of the target. In fact, in IJD, a pulsed electron source is used in vacuum to generate ultra-short electric discharges in the megawatt range (voltage pulse amplitude up to 25 kV, duration lower than 1 μs). The discharge is supported by a gas jet and is directed towards the target using a trigger combined with auxiliary electrodes. This generates a superficial explosion with the consequent emission and ionization of the material and the formation of the plasma plume [50,51]. Because of the characteristics of the ablation source and of the deposition procedure, IJD permits a higher efficiency and a better stoichiometry conservation compared to pulsed plasma deposition and pulsed electron deposition [50], also for complex compounds (superconducting oxides or photoactive semiconductors), as in the case of PLD. However, it has been reported that ablation of metals by PED and IJD can be complicated by their high thermal conductivity, that tends to dissipate the beam energy in the bulk target [52–54]. Hence, here different thermal conductivity between Ag and TCP can explain the lower presence of silver in the films. However, conservation of the amount of silver in the coating can be considered fair, and it is close to values used in the literature [30–32], hence it is expected to provide suitable antibacterial efficacy.

In spite of the slight difference in concentration compared to the target, in Ag-TCP-30, silver is detected in all areas of the sample, with some variability among different zones. For samples at lower deposition time, instead, heterogeneity in Ag content appears very high. Even though some variability can be ascribed to irregularity in the surface morphology and depth profile (sample Ag-TCP-20) and to low thickness (Ag-TCP-10) interfering with Ag detection by EDS, still the sample Ag-TCP-30 is preferred, as it is the only one exhibiting suitable Ag content and low variability.

Differently from the Ag content, the Ca/P ratio is comparable for all the three conditions. For Ag-TCP-30, a Ca/P ratio of 1.57 ± 0,06 [at.%] has been found, very close to the stoichiometric value for TCP (1,5 at.%), indicating that TCP is by far the main phase in the coatings. The slight increase in the Ca/P ratio with respect to the stoichiometric value confirms possible formation of some carbonated hydroxyapatite, detected by FT-IR.

The obtained data indicate that, when appropriate parameters are selected, deposition of Ag-TCP by IJD permits to preserve both the main calcium phosphate phase and silver doping, obtaining highly homogeneous nanostructured films, as required. Based on the Ag content and uniformity in morphology and thickness, the Ag-TCP-30 min sample is selected and subjected to further characterization.

Vickers microindentation was used to test hardness of the Ag-TCP film. The measured hardness was that of the film-substrate composite system. The obtained data are plotted versus the inverse imprint diagonal and are presented in Fig. 5b. Taking into-account the film's thickness of about 300 nm, the intrinsic film hardness can be extracted, and is found to be 24 ± 6 GPa. In lit. ref [55], microhardness of TCP coatings deposited on Ti-6Al-4V was investigated. For film's thickness ranging from 400 to 1000 nm, a hardness value ranging from 4.2 to 4.6 GPa was reported. In this work, the hardness value obtained for the Ag-TCP coating is significantly higher (24 GPa), evidencing good mechanical properties of the coatings. Likely, the Ag substitution contributes to the enhanced hardness.

Dissolution profile of the coatings at different timepoints is shown in Fig. 6.

Images after 1, 7 and 14 days of immersion in alpha-MEM clearly show that the film is still present on the Ti substrate (Fig. 6 a-i), indicating that the coating does not experience too fast a dissolution, that would result into excessive ion release, interfering with cells viability [56]. As the immersion proceeds, the coating appears more flat, aggregates dimensions tend to decrease and the surface finishing of the implant becomes increasingly visible, indicating that the films become thinner. Between 14 and 20 days of immersion, the coating experiences significant dissolution, so that at the latest timepoint it is almost completely dissolved, even though the presence of fine aggregates is still visible at the highest magnifications (Figure 6l). Presence of the coating is confirmed by the signals of Ca, P and Mg in the EDS spectra (Fig. S4). This is compatible with the dynamics desired for dissolution of the coatings, hence indicating that films show a suitable stability profile. In fact, it is generally required that antibacterial coatings can guarantee a burst release of the antibacterial agents, to prevent infection in the hours following surgery (≈48h). To permit such a high solubility, TCP was selected over a less soluble HA. In the following days, release shall progressively decrease as the coating progressively dissolves, to avoid interference with bone regeneration. However, if the coating is capable of avoiding interference with cells differentiation, a longer dissolution time-frame is recommended (at least 14–21 days), so that it can be active also against a late infection.

Here, importantly, a progressive dissolution results into a flattening of the coating morphology and a progressively reduced thickness (Fig. 6b,f,h,k), but does not cause cracking or detachment of fragments, that could cause inflammation or excessive toxicity upon implantation *in vivo*.

The effect of TCP and Ag-TPC on the planktonic growth of different microorganisms (*C. albicans, E. faecalis, S. aureus, E. coli* and *P. aeruginosa*) was assessed by measuring OD_{600} after 24 h of incubation at optimal growth temperatures (Fig. 7). For each microorganism, the inhibition caused by the Ag-TCP was calculated from the percentage of growth with respect to the TCP coating and to the control (Table 2).

This test shows that the planktonic growth of all microorganisms slightly increases in the presence of the TCP coatings, as their OD is greater than that of the positive controls. This increase is consistent with literature studies that showed that morphological features that favor host cells adhesion (such as porosity, high roughness and nanostructuration), including nanostructured surface morphology of the coatings, can also favor microbial colonization [57], further increasing the need for antimicrobial coatings. The presence of conditions favouring growth under adhesion conditions might positively influence also the planktonic growth, which enters in an equilibrium state with the biofilm [58]. In our experiments, the difference between control sample and TCP is visible but not statistically significant for the strains of *E. coli*, *S. aureus*, C. *albicans* and *E. faecalis*. Conversely, the TCP nanostructuration results to have a strong positive influence on the growth of *P. aeruginosa* (Fig. 7), whereas the presence of silver in the coating (Ag-TCP) significantly reduces the optical density of this strain by 18.5% when compared to the pure TCP condition. Furthermore, the presence of silver in the coating exerts a strain-specific antimicrobial activity against *E. coli, S. aureus,* and *C. albicans*, that is associated with a significant decrease of the planktonic growth of these strains when Ag-TCP condition is compared to both TCP and the control. This indicates that, for these strains, the antimicrobial effect of the incorporation of silver dominates on that of nanostructuration.

The capability of Ag-TCP to prevent bacterial cell adhesion was also investigated (Fig. 8). The obtained results demonstrate a significant decrease in the amount of attached cells for all the four tested bacteria with respect to pure TCP. In particular, the capacity of attachment of the two Gram negative strains *E. coli* and *P. aeruginosa* to the coatings revealed a higher sensitivity to the presence of silver, with anti-adhesion activity reduced up to 69.9% and 59.0% respectively, as compared to the two Gram positive bacteria *S. aureus* and *E. faecalis* (anti-adhesion activity reduced up to 26.0% and 50.2%, respectively). Reduction of bacterial adhesion is expected to have a significant impact on the reduction of biofilm formation *in vitro* and *in vivo*, as it is the first and essential stage of biofilm formation. These data are in agreement with

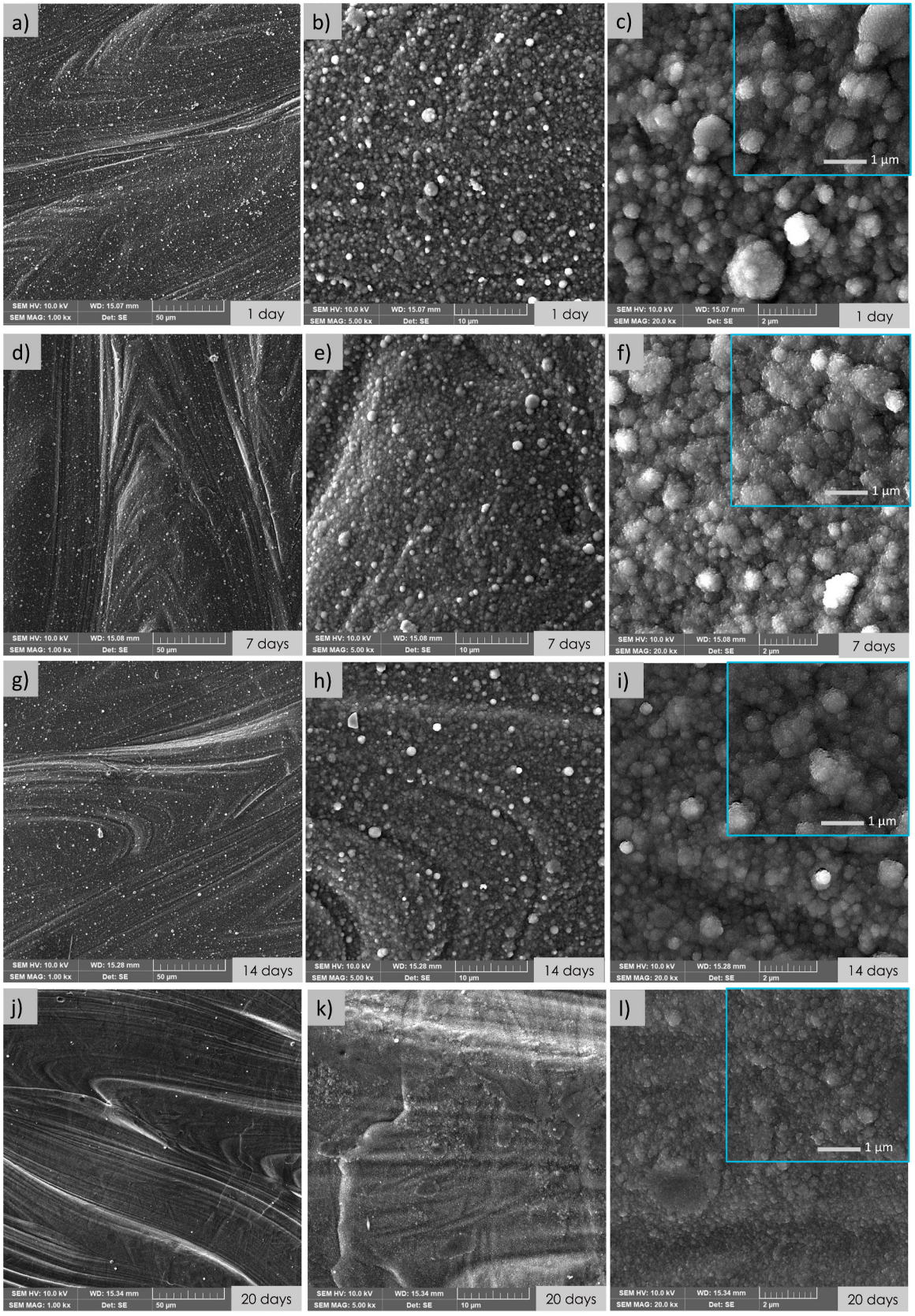

Fig. 6. Morphology of the Ag-TCP-30 coating after (a–c) 1 day, (d–f) 7 days, (g–i) 14 days and (j,l) 20 days immersion in the medium. Coating presence is evident up to 14 days of immersion (a–i). After 20 days, the coating seems to be completely dissolved (j,k), but images at higher magnification (l) show that the aggregates are still present, though significantly smaller. No cracking or detachments are visible for any of the examined immersion times (a,d,g,j). A progressive reduction of film thickness is suggested by the increasing visibility of surface finishing of the substrate at 5.000× magnification (b,e,h,k).

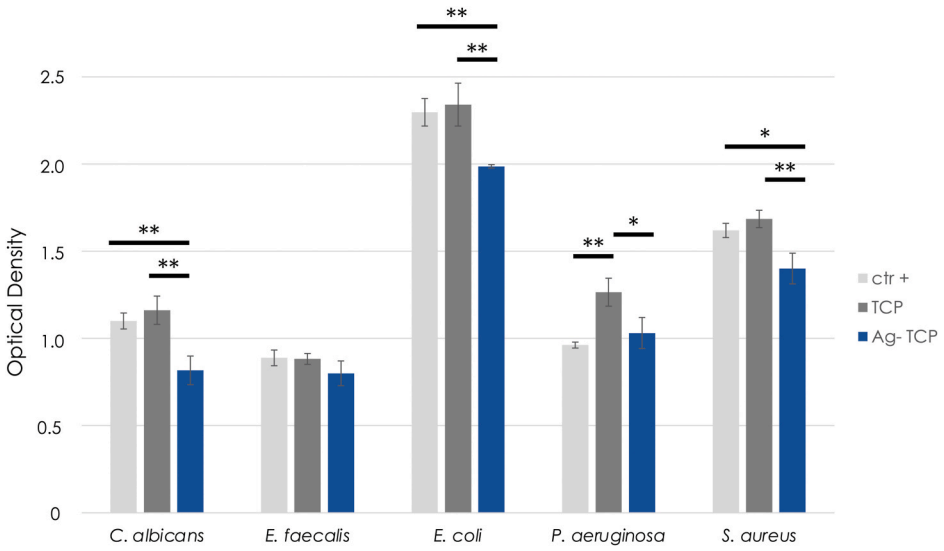

Fig. 7. Results of antimicrobial tests indicated as OD_{600} of the cultures of four bacterial pathogens and *C. albicans* fungus on Ti plates in the presence and absence (CTR-control) of Ag-TCP (Ag-TCP-30) or TCP The average OD_{600} and the standard deviation (SD) are reported deriving from three independent experiments. Statistically significant differences are indicated with * ($p < 0.05$) and ** ($p < 0.01$).

Table 2
Percentage of inhibition for the different microorganisms. Asterisks indicate: *, $p < 0.05$; **, $p < 0.01$.

	C. albicans	*E. faecalis*	*E. coli*	*P. aeruginosa*	*S. aureus*
% inhibition (Ag-TCP vs TCP)	29.7**	9.4	15.1**	18.5*	16.9**
% inhibition (Ag-TCP vs control)	25.7**	10.0	13.5**	−7.2	13.5*

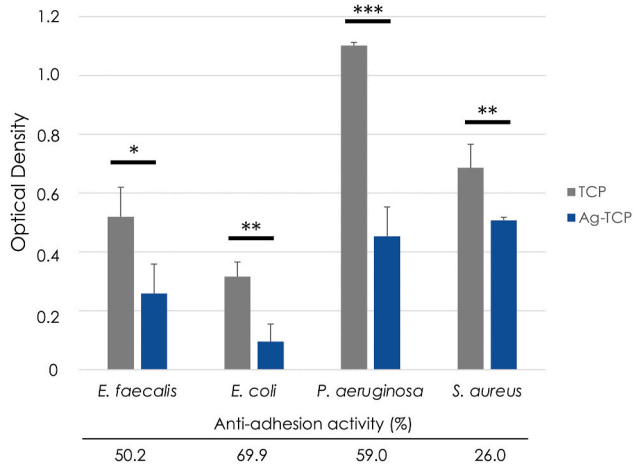

Fig. 8. Ag-TCP anti-adhesive performance compared to TCP in the presence of four different bacterial pathogens. The amount of adhered bacterial cells was quantified by crystal violet staining and absorbance measurements at 595 nm. Bars represent means ± standard deviations. Statistically significant differences are indicated with * ($p < 0.05$), ** ($p < 0.01$) and *** ($p < 0.001$).

the higher efficacy of silver on Gram negative strains, generally reported in the literature. However, interestingly, a significant effect is assessed on both the Gram positive *S. aureus* and the Gram negative *E. coli* strains, which are the most relevant bacteria in orthopedic infection. In conclusion, these silver-containing coatings exhibited antimicrobial activity of 15–30% against most of the microbial strains tested and minimized the bacterial adhesion of all strains, which is the initial step of biofilm formation. These features encourage the further optimizations to boost their possible applicability in orthopaedical implants.

To study the effect of Ag-TCP on ADMSC, the MTT test was performed after 24 h of ADMSC growth in the absence and presence of TCP and Ag-TCP-30. Results are shown in Fig. 9a, expressed as percentage of viability, and in Fig. S5, expressed as optical density. Fig. 9a shows readings of the formazan produced by the ADMSCs incubated alone (control sample) and with TCP and Ag-TCP. As can be seen from Fig. 9a, there is a positive effect of the nanostructured TCP coatings on cells number and viability, both in the absence (+12,6% viability, compared to control) and in the presence of silver (+9,7% viability). This indicates not only that the coatings are non-cytotoxic, but also that the combined effect of bioactive composition and nanostructured surface morphology can favor cells viability and completely mitigate possible negative effects of silver.

Fig. 9b qualitatively shows the ADMSCs grown in osteogenic medium on plastic (positive control) (d) and when cultured with TCP and Ag-TCP coatings (b and c, respectively). To show possible impairment of osteogenic differentiation, results are compared to ADMSCs in growth medium, used as a negative control (d). Osteogenic differentiation is evident from the red colour of the extracellular matrix obtained in the differentiation, absent in the negative control. In particular, red staining of the extracellular matrix is maximum for the TCP samples and is comparable for the Ag-TCP and positive control. This indicates that TCP and Ag-TCP do not negatively affect the ADMSCs differentiation towards the osteogenic lineage. Results of the MTT and Alizarine Red tests indicate that no cytotoxic effect is caused by silver-substituted films.

The results obtained from biological tests, although preliminary, indicate that the coatings can exert a marked antibacterial and antimycotic effect without causing cytotoxicity or interfering with the capability of cells to differentiate towards an osteogenic lineage. Instead, because of the use of bioactive β-TCP and surface nanostructuration, films permit high cells viability, which indicates a potential positive effect on bone regeneration, that will be further explored in future studies. More in detail, studies are currently in progress to better investigate the interactions between the coatings and host cells, in terms of adhesion and proliferation, viability at early and late timepoints (24h, 72h, 7 days) and of direct differentiation assays.

In the literature, antibacterial silver films have been proposed and their efficacy has been demonstrated against *P. aeruginosa* and *E. coli* (for coatings manufactured by electrodeposition [31]) and against *S. aureus*

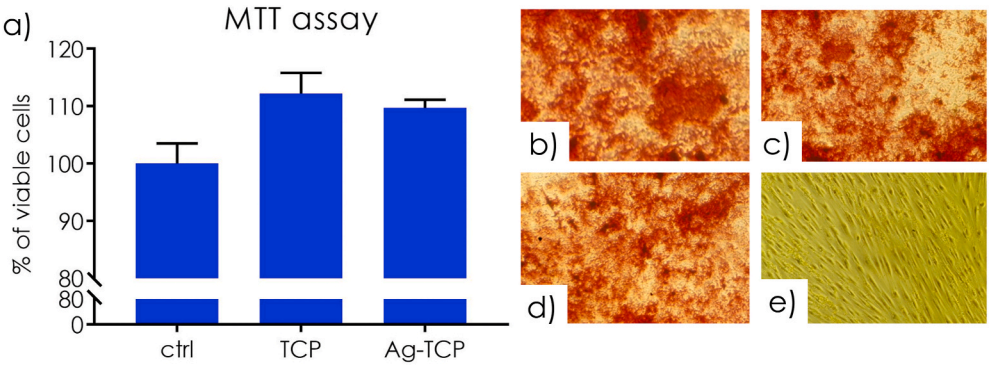

Fig. 9. a) MTT test. ADMSC viability after 24 h without (positive control) and with TCP and Ag-TCP. The experiment was repeated in triplicate. b-e) Qualitative evaluation of the osteogenic differentiation of ADMSC at 21 days by Alizarin Red S staining. (b) TCP samples in the presence of osteogenic differentiation medium, (c) Ag-TCP samples in the presence of osteogenic differentiation medium, (d) ADMSC with osteogenic differentiation medium (positive control) and (e) ADMSC without osteogenic differentiation medium (negative control). Magnification 20×.

and *E. coli* (for coatings produced by micro-arch deposition [32]), evaluated in terms of reduction of bacterial viability caused by the coatings [31] or their eluates [32]. In this work, efficacy against *E. coli* and *S. aureus* has been reached for lower concentration of silver in the coating and much lower thickness (≈300 nm vs ≈ 150 μm in Ref. [31]). A slight effect, although non-statistically significant, has been highlighted on *E. faecalis* (Fig. 7, Table 2), pushing towards an optimization for this strain. This higher efficacy for lower silver content shall be ascribed to nanostructuration, as the reported references propose coatings having features at the micro-scale.

Remarkable efficacy has been shown against fungus *C. albicans* (Fig. 7, Table 2), indicating that Ag-TCP films can have promising applications also in the prevention of fungal growth. Even though it is a less investigated issue compared to bacterial infection due to lower incidence rate, fungal infection still represents about 1% of periprosthetic joint infections (PJI), the majority of which are caused by *Candida albicans*. In addition, in spite of a relatively low incidence, fungal infection is particularly hard to treat, due to its persistence and high tendency to relapse [59,60]. For this reason, international guidelines for treatment (Infectious Disease Society of America – IDSA and European Society for Clinical Microbiology and Infectious Diseases - ESCMID) recommend surgical debridement combined with prolonged (6–12 months) systemic therapy [60]. As a consequence, both in case of bacterial and fungal infection, since the treatment is challenging, prevention should be preferred. Notably, among multiple potential risk factors for the development of fungal infection, immunosuppression and chronic or prolonged use of antibiotics are reported [60], thus indicating that the use of multi spectrum compounds having both antibacterial and antifungal activity is particularly promising, as it allows decreasing the need for antibiotics.

Together with the reduction of bacterial viability, here we show that the Ag-TCP film can positively impact on addressing infection by reducing the adhesion of all the examined bacterial strains (Fig. 8). This aspect is important, because adhesion is a crucial step in biofilm formation, hence these results indicate that the study of reduction of bacterial adhesion by application of nanostructured Ag-substituted TCP films is worth to be further investigated, also for coatings manufactured by alternative techniques. The study of the possible influence of silver on the reduction of cells adhesion also appears to be promising, and is currently under investigation.

Although a further investigation is needed to fully investigate the interactions between the thin films and host cells, the results obtained in this work indicate that the prepared coatings are non-cytotoxic and do not negatively impact on cell differentiation (Fig. 9b–e). Interestingly, nanostructuring of the films seems to have an important impact on their toxicity. In fact, when coatings features are micrometric, a decrease is reported in cells viability for increasing surface roughness [32]. Here, instead, a positive effect of roughness at the nanoscale is suggested (Fig. 9a), also for antibacterial films. The latter aspect had not been yet investigated in the literature for Ag-TCP films, as the studies were focused on cells viability and proliferation. The submicrometric thickness of the films is also important, as inflammation and toxicity phenomena have been reported for silver coated prostheses *in vitro* and *in vivo* [61,62], caused by an excessive silver release and by the detachment of silver fragments from the film. Cracking and detachments, in turn, can occur as a consequence of mechanical mismatch between the coating and the implant, resulting from excessive thickness. Here, we demonstrate that the coatings proposed in this work are homogeneous and do not show defects or cracking, not even after immersion in the physiological solution medium. In fact, the coatings progressively dissolve without causing cracking or scaling, hence indicating that this issue will not be a concern, for perspective application *in vivo*.

4. Conclusions

Nanostructured antibacterial thin films were successfully deposited by IJD starting from Ag-TCP (0.11 wt%) targets. The produced films meet all the challenges highlighted for the development of antibacterial coatings, regarding composition, surface morphology and surface roughness, absence of defects, submicrometric thickness, and high reproducibility. In fact, the deposited Ag-TCP films are composed of β-TCP phase and Ag (0.08 wt%) and have a nanostructured surface morphology, high surface roughness (RMS ranging from 52 ± 6 nm, to 69 ± 27 nm and 78 ± 16 nm for deposition times of 10, 20 and 30 min, respectively) and submicrometric thickness (301 ± 45 nm for the optimized condition, i.e. for 30 min deposition on titanium). Thanks to the characteristics of IJD, the stoichiometry of the target material is maintained in the deposited coatings. This is achieved without the need for heating the substrate, indicating that the coatings can be easily applied to several biomedical devices for orthopedic use.

Both deposition time and substrate morphology and composition significantly impact on the characteristics of the coatings, as they determine the dimensions and the distribution of the globular aggregates that constitute them (22 ÷ 980 nm diameter), the overall roughness and their thickness. In fact, increasing deposition time results into the formation of larger clusters of nanosized aggregates, higher surface homogeneity, higher roughness and increased thickness. As a consequence, selection of the deposition duration is an essential task to be optimized for each substrate under investigation. For the selected deposition conditions, 30 min was found to be the optimal deposition duration.

The deposited coatings show suitable mechanical properties, as an intrinsic film hardness of 24 ± 6 GPa, was measured, which is consistently higher than that reported in the literature for TCP films.

Different from what found in the literature for bone apatite and hydroxyapatite films deposited by IJD at room temperature, a good stability and dissolution profile are found. In fact, the films progressively dissolve without causing detachments and remain present after over 20 days in medium.

The results of biological tests indicate that silver ions are released in

a concentration suitable to impart antimicrobial properties to the deposited coatings. In particular, the coatings were found to be effective in the inhibition of the planktonic growth of Gram positive and Gram negative bacteria (*E. coli, S. aureus*) and fungus *C. albicans.* Further tests will be carried out at higher Ag substitution contents, to further enhance the antimicrobial capacity of the coatings towards *E. faecalis* and *P. aeruginosa*. However, for all the examined strains, including *E. faecalis* and *P. aeruginosa*, a significant decrease is found in bacterial cells' adhesion, that is maximum for the two Gram negative species. Impeded adhesion is a key step in the prevention of biofilm formation, that will be further investigated.

For ADMSCs, no cytotoxicity was assessed, as TCP and Ag-TCP films increase cells' viability and do not interfere with their capability to differentiate towards an osteogenic lineage.

Therefore, the Ag-TCP coatings appear promising for application in orthopedic implants.

CRediT authorship contribution statement

Gabriela Graziani: Conceptualization, Methodology, Investigation, Validation, Formal analysis, Resources, Writing - original draft, Project administration, Funding acquisition, Supervision. **Katia Barbaro:** Methodology, Investigation, Validation, Formal analysis, Writing - review & editing. **Inna V. Fadeeva:** Methodology, Investigation, Validation, Formal analysis, Writing - review & editing. **Daniele Ghezzi:** Methodology, Investigation, Validation, Formal analysis, Writing - review & editing. **Marco Fosca:** Methodology, Investigation, Validation, Formal analysis, Writing - review & editing. **Enrico Sassoni:** Methodology, Investigation, Validation, Formal analysis, Writing - review & editing. **Gianluca Vadalà:** Supervision, Writing - review & editing. **Martina Cappelletti:** Methodology, Investigation, Validation, Formal analysis, Writing - review & editing. **Francesco Valle:** Methodology, Investigation, Validation, Formal analysis, Writing - review & editing. **Nicola Baldini:** Supervision, Funding acquisition, Project administration, Writing - review & editing. **Julietta V. Rau:** Conceptualization, Methodology, Investigation, Validation, Formal analysis, Resources, Writing - original draft, Project administration, Funding acquisition, Supervision, Writing - review & editing.

Declaration of competing interest

The Authors declare no conflict of interest.

Acknowledgements

Dr. Gabriela Graziani acknowledges funding from the project Starting Grant SG-2018-12367059, financed by the Italian Ministry of Health (BANDO RICERCA FINALIZZATA 2018).

The technical assistance of Mr. Luca Imperatori, Mr. Marco Ortenzi, Mr. Massimo Di Menno Di Bucchianico, Mr. Agostino Nana and Dr. Francesca Ospitali is gratefully acknowledged. Dr. Giorgia Borciani is acknowledged for support in dissolution tests.

Appendix A. Supplementary data

Supplementary data to this article can be found online at https://doi.org/10.1016/j.bioactmat.2020.12.019.

References

[1] M. Vafa Homann, et al., Improved ex vivo blood compatibility of central venous catheter with noble metal alloy coating, J. Biomed. Mater. Res. B Appl. Biomater. 104 (7) (2016) 1359–1365.
[2] W.R. Fordham, et al., Silver as a bactericidal coating for biomedical implants, Surf. Coating. Technol. 253 (2014) 52–57.
[3] V. Alt, Antimicrobial coated implants in trauma and orthopaedics-A clinical review and risk-benefit analysis, Injury 48 (2017) 599–607.
[4] P.I. Branemark, Introduction to Osseointegration, Quintessence Publishing Co., 1985, pp. 11–76.
[5] J. Raphel, M. Holodniy, S.B. Goodman, S.C. Heilshorn, Multifunctional coatings to simultaneously promote osseointegration and prevent infection of orthopaedic implants, Biomaterials 84 (2016) 301–314.
[6] A. De Bonis, V. Uskokovic, K. Barbaro, I. Fadeeva, M. Curcio, L. Imperatori, R. Teghil, J.V. Rau, Pulsed laser deposition temperature effects on strontium-substituted hydroxyapatite thin films for biomedical implants, Cell Biol. Toxicol. (2020), https://doi.org/10.1007/s10565-020-09527-3.
[7] K.A. Prosolov, M.A. Khimich, J.V. Rau, D.V. Lychagin, Y.P. Sharkeev, Influence of oblique angle deposition on Cu-substituted hydroxyapatite nano-roughness and morphology, Surf. Coating. Technol. 394 (2020), 125883.
[8] K.A. Prosolov, O.A. Belyavskaya, J. Linders, K. Loza, O. Prymak, C. Mayer, J. V. Rau, M. Epple, Y.P. Sharkeev, Glancing angle deposition of Zn-doped calcium phosphate coatings by RF magnetron sputtering, Coatings 9 (2019) 220.
[9] J.V. Rau, I. Cacciotti, A. De Bonis, M. Fosca, V. Komlev, A. Latini, A. Santagata, R. Teghil, Fe-doped hydroxyapatite coatings for orthopaedic and dental implant applications, Appl. Surf. Sci. 307 (2014) 301–305.
[10] J.V. Rau, V.V. Smirnov, S. Laureti, A. Generosi, G. Varvaro, M. Fosca, D. Ferro, S. Nunziante Cesaro, V. Rossi Albertini, S.M. Barinov, Properties of pulsed laser deposited fluorinated hydroxyapatite films on titanium, Mater. Res. Bull. 45 (2010) 1304–1310.
[11] J.V. Rau, I. Cacciotti, S. Laureti, M. Fosca, G. Varvaro, A. Latini, Bioactive, nanostructured Si-substituted hydroxyapatite coatings on titanium prepared by pulsed laser deposition, J. Biomed. Mater. Res. B Appl. Biomater. 103 (8) (2015) 1621–1631.
[12] L. Clèries, J.M. Fernández-Pradas, G. Sardin, J.L. Morenza, Application of dissolution experiments to characterise the structure of pulsed laser-deposited calcium phosphate coatings, Biomaterials 20 (1999) 1401–1405.
[13] H.P. Lim, S.W. Park, K.D. Yun, C. Park, M.K. Ji, G.J. Oh, J.T. Lee, K. Lee, Novel beta-TCP coated titanium nanofiber surface for enhanced bone growth, J. Nanosci. Nanotechnol. 18 (2) (2018) 853–855.
[14] S.I. Goreninskii, N.N. Bogomolova, A.I. Malchikhina, et al., Biological effect of the surface modification of the fibrous poly(L-lactic acid) scaffolds by radio frequency magnetron sputtering of different calcium-phosphate targets, BioNanoSci 7 (2017) 50.
[15] K.R. Kang, Z.G. Piao, J.S. Kim, I.A. Cho, M.J. Yim, B.H. Kim, J.S. Oh, J.S. Son, C. S. Kim, D.K. Kim, S.Y. Lee, S.G. Kim, Synthesis and electrochemical characterization a coating of beta-tricalcium phosphate deposited on steel 316LVM, Implant Dent. 26 (3) (2017) 378–387.
[16] V. Uskoković, V. Graziani, V.M. Wu, I.V. Fadeeva, A.S. Fomin, I.A. Presniakov, M. Fosca, M. Ortenzi, R. Caminiti, J.V. Rau, Gold is for the mistress, silver for the maid: enhanced mechanical properties, osteoinduction and antibacterial activity due to iron doping of tricalcium phosphate bone cements, Mater Sci Eng C Mater Biol Appl 94 (2019) 798–810.
[17] J.V. Rau, M. Fosca, V. Graziani, et al., Silver-doped calcium phosphate bone cements with antibacterial properties, J. Funct. Biomater. 7 (2) (2016) 10.
[18] A. Ewald, D. Hösel, S. Patel, L.M. Grover, J.E. Barralet, U. Gbureck, Silver-doped calcium phosphate cements with antimicrobial activity, Acta Biomater. 7 (11) (2011) 4064–4070.
[19] I.V. Antoniac, M. Filipescu, K. Barbaro, A. Bonciu, R. Birjega, C.M. Cotrut, E. Galvano, M. Fosca, I.V. Fadeeva, G. Vadalà, M. Dinescu, J.V. Rau, Iron ion doped tricalcium phosphate coatings improve the properties of biodegradable magnesium alloys for biomedical implant application, Adv. Mater. Interfaces 7 (16) (2020), 2000531.
[20] R.A. Surmenev, A review of plasma-assisted methods for calcium phosphate-based coatings fabrication, Surf. Coating. Technol. 206 (2012) 2035–2056.
[21] R.A. Surmenev, M.A. Surmeneva, A.A. Ivanova, Significance of calcium phosphate coatings for the enhancement of new bone osteogenesis – a review, Acta Biomater. 10 (2014) 557–579.
[22] S.V. Dorozhkin, Calcium orthophosphate coatings, films and layers, Prog. Biometeorol. 1 (2012) 1.
[23] Y. Yang, K.H. Kim, J.L. Ong, A review on calcium phosphate coatings produced using a sputtering process-an alternative to plasma spraying, Biomaterials 26 (2005) 327–337.
[24] M.B. Sedelnikova, E.G. Komarova, Y.P. Sharkeev, A.V. Ugodchikova, T. V. Tolkacheva, J.V. Rau, E.E. Buyko, V.V. Ivanov, V.V. Sheikin, Modification of titanium surface via Ag-, Sr- and Si-containing micro-arc calcium phosphate coating, Bioactive Mater. 4 (2019) 224–235.
[25] G. Socol, M. Socol, L.E. Sima, S. Petrescu, M. Enculescu, F. Sima, M. Miroiu, G. Popescu-Pelin, N. Stefan, R. Cristescu, C.N. Mihailescu, A. Stanculescu, C. Sutan, I.N. Mihailescu, Combinatorial pulsed laser deposition of Ag-containing calcium phosphate coatings, Digest J. Nanomater. Biostruct. 7 (2) (2012) 563–576.
[26] P. Rajesh, C.V. Muraleedharan, S. Sureshbabu, M. Komath, H. Varma, Preparation and analysis of chemically gradient functional bioceramic coating formed by pulsed laser deposition, J. Mater. Sci. Mater. Med. 23 (2) (2012) 339–348.
[27] F. Sima, G. Socol, E. Axente, I.N. Mihailescu, L. Zdrentu, S.M. Petrescu, I. Mayer, Biocompatible and bioactive coatings of Mn2+-doped beta-tricalcium phosphate synthesized by pulsed laser deposition, Appl. Surf. Sci. 254 (2007) 1155–1159.
[28] W. Mróz, M. Jedyński, A. Prokopiuk, A. Ślósarczyk, Z. Paszkiewicz, Characterization of calcium phosphate coatings doped with Mg, deposited by pulsed laser deposition technique using ArF excimer laser, Micron 40 (2009) 140–142.
[29] R. Kotoka, N.K. Yamoah, K. Mensah-Darkwa, T. Moses, D. Kumar, Electrochemical corrosion behavior of silver doped tricalcium phosphate coatings on magnesium for biomedical application, Surf. Coating. Technol. 292 (2016) 99–109.

[30] I.V. Fadeeva, V.I. Kalita, D.I. Komlev, A.A. Radiuk, A.S. Fomin, G.A. Davidova, N. K. Fursova, F.F. Murzakhanov, M.R. Gafurov, M. Fosca, I.V. Antoniac, S. M. Barinov, J.V. Rau, In vitro properties of manganese-substituted tricalcium phosphate coatings for titanium biomedical implants deposited by arc plasma, Materials 13 (19) (2020) 4411.
[31] M. Roy, A. Bandyopadhyay, S. Bose, In vitro antimicrobial and biological properties of laser assisted tricalcium phosphate coating, Mater Sci Eng C Mater Biol Appl 29 (6) (2009) 1965–1968.
[32] W.H. Song, H.S. Ryu, S.H. Hong, Antibacterial properties of Ag (or Pt)-containing calcium phosphate coatings formed by micro-arc oxidation, J. Biomed. Mater. Res. 88 (1) (2009) 246–254.
[33] G. Graziani, M. Berni, A. Gambardella, M. De Carolis, M.C. Maltarello, M. Boi, G. Carnevale, M. Bianchi, Fabrication and characterization of biomimetic hydroxyapatite thin films for bone implants by direct ablation of a biogenic source, Mater. Sci. Eng. C 99 (2019) 853–862.
[34] M. Bianchi, L. Degli Esposti, A. Ballardini, A. Tampieri, M. Iafisco, Strontium doped calcium phosphate coatings on poly(etheretherketone) (PEEK) by pulsed electron deposition, Surf. Coating. Technol. 319 (2017) 191–199.
[35] D. Bellucci, M. Bianchi, G. Graziani, A. Gambardella, M. Berni, A. Russo, V. Cannillo, Pulsed Electron Deposition of nanostructured bioactive glass coatings for biomedical applications, Ceram. Int. 43 (2017) 15862–15867.
[36] M. Bianchi, A. Pisciotta, L. Bertoni, M. Berni, A. Gambardella, A. Visani, A. Russo, A. de Pol, G. Carnevale, Osteogenic differentiation of hDPSCs on biogenic bone apatite thin films, Stem Cell. (2017), 3579283.
[37] G. Pagnotta, G. Graziani, et al., Nanodecoration of electrospun polymeric fibers with nanostructured silver coatings by ionized jet deposition for antibacterial tissues, Mater. Sci. Eng. C 113 (2020), 110998.
[38] F. Valle, et al., Nanoscale morphological analysis of soft matter aggregates with fractal dimension ranging from 1 to 3, Micron 100 (2017) 60–72.
[39] D. Ferro, S.M. Barinov, J.V. Rau, A. Latini, R. Scandurra, B. Brunetti, Vickers and Knoop hardness of electron beam deposited ZrC and HfC thin films on titanium, Surf. Coating. Technol. 200 (16–17) (2006) 4701–4707.
[40] G. Renaudin, S. Gomes, J.M. Nedelec, First-row transition metal doping in calcium phosphate bioceramics: a detailed crystallographic study, Materials 10 (1) (2017), 92. 2.
[41] K. Sanjeevi, I. Lemos, J. Rocha, J. Ferreira, Synthesis and characterization of magnesium substituted biphasic mixtures of controlled hydroxyapatite/tricalcium phosphate ratios, J. Solid State Chem. 178 (2005) 3190–3196, 2005.
[42] A. Gambardella, M. Berni, A. Russo, M. Bianchi, A comparative study of the growth dynamics of zirconia thin films deposited by ionized jet deposition onto different substrates, Surf. Coating. Technol. 337 (2018) 306–312.
[43] X. Liu, Micro/nano-structured TiO2 surface with dual-functional antibacterial effects for biomedical applications, Bioact Mater 4 (2019) 346–357.
[44] G.M. de Peppo, Osteogenic response of human mesenchymal stem cells to well-defined nanoscale topography in vitro, Int. J. Nanomed. 9 (1) (2014) 2499–2515.
[45] Y. Hou, L. Yu, W. Xie, L.C. Camacho, M. Zhang, Z. Chu, Q. Wei, R. Haag, Surface roughness and substrate stiffness synergize to drive cellular mechanoresponse, Nano Lett. 20 (1) (2020) 748–757.
[46] M.B. Berger, Human osteoblasts exhibit sexual dimorphism in their response to estrogen on microstructured titanium surfaces, Biol. Sex Differ. 9 (1) (2018) 3.
[47] A.S.G. Curtis, Nanotechniques and approaches in biotechnology, Trends Biotechnol. 19 (2001) 97–101.
[48] M.J. Dalby, Osteoprogenitor response to defined topographies with nanoscale depth, Biomaterials 27 (8) (2006) 1306–1315.
[49] G. Graziani, et al., A Comprehensive microstructural and compositional characterization of allogenic and xenogenic bone: application to bone grafts and nanostructured biomimetic coatings, Coatings 10 (6) (2020) 522.
[50] A. Liguori, C. Gualandi, M.L. Focarete, F. Biscarini, M. Bianchi, The pulsed electron deposition technique for biomedical applications: a review, Coatings 10 (2020) 16.
[51] L. Skocdopolova, Device For Generating Plasma And Directing An Electron Beam Towards A Target, 25 December 2013. WO Patent 2013/186697.
[52] M. Strikovski, K.S. Harshavardhan, Parameters that control pulsed electron beam ablation of materials and film deposition processes, Appl. Phys. Lett. 82 (2003) 853–855.
[53] M. Nistor, N.B. Mandache, J. Perrière, Pulsed electron beam deposition of oxide thin films, J. Phys. D 41 (2008) 175205–175215.
[54] G. Close, M. Müller, G. Konijnenberg, C. Krafft, Schultheiss Thin film deposition by means of pulsed electron beam ablation, Sci. Technol. Thin Film (1995) 89–119.
[55] R.R. Behera, A. Das, D. Pamu, L.M. Pandey, M.R. Sankar, Mechano-tribological properties and in vitro bioactivity of biphasic calcium phosphate coating on Ti-6Al-4V, J. Mech. Behav. Biomed. Mater. 86 (2018) 143–157.
[56] M. Bianchi, et al., Plasma-assisted deposition of bone apatite-like thin films from natural apatite, Mater. Lett. 199 (2017) 32–36.
[57] M. Lorenzetti, I. Dogša, T. Stošicki, D. Stopar, M. Kalin, S. Kobe, S. Novak, The influence of surface modification on bacterial adhesion to titanium-based substrates, ACS Appl. Mater. Interfaces 7 (3) (2015) 1644–1651.
[58] E. Bester, et al., Biofilms' role in planktonic cell proliferation, Int. J. Mol. Sci. 14 (11) (2013) 21965–21982.
[59] A.O. Miller, M.N. Gamaletsou, M.W. Henry, L. Al-Hafez, K. Hussain, N.V. Sipsas, D. P. Kontoyiannis, E. Roilides, B.D. Brause, T.J. Walsh, Successful treatment of Candida osteoarticular infections with limited duration of antifungal therapy and orthopedic surgical intervention, Inf. Disp. 47 (3) (2015) 144–149.
[60] B. Schoof, O. Jakobs, S. Schmidl, T.O. Klatte, L. Frommelt, T. Gehrke, M. Gebauer, Fungal periprosthetic joint infection of the hip: a systematic review, Orthop. Rev. 7 (1) (2015) 5748.
[61] G. Goshegera, et al., Silver-coated megaendoprostheses in a rabbit model—an analysis of the infection rate and toxicological side effects, Biomaterials 25 (24) (2004) 5547–5556.
[62] C. Moseke, et al., Hard implant coatings with antimicrobial properties, J. Mater. Sci. Mater. Med. 22 (12) (2011 Dec) 2711–2720.